

# Micromechanical Modeling and Design Optimization of 2-D Triaxial Braided Composites

John T. Hwang <sup>\*</sup>, Anthony M. Waas <sup>†</sup>, Joaquim R. R. A. Martins <sup>‡</sup>

*University of Michigan, Ann Arbor, Michigan, 48109, United States*

A micromechanical model for 2-D triaxial braided composites is presented. The tow arrangement in the representative unit cell is modeled by solving the packing problem using analytical optimization, avoiding the need to measure the geometric properties experimentally. These results are used in the development of a closed-form micromechanical model predicting the full 3-D stiffness matrix of the homogenized representative unit cell. The results show good agreement with experimental data; however, the true significance of this work is that it enables design optimization using 2-D triaxial braided composites because the need for experimental calibration for each set of design variables is eliminated.

## Nomenclature

$\mathcal{F}^*$	$\{x^*, y^*, z^*\}^T$	Plate frame
$\mathcal{F}$	$\{x, y, z\}^T$	Unit cell frame
$\mathcal{F}'$	$\{x', y', z'\}^T$	In-plane tow frame
$\mathcal{F}''$	$\{x'', y'', z''\}^T$	Undulated tow frame
$A_a, A_b$		Tow area
$\tilde{A}_a, \tilde{A}_b$		Tow area projected along the other tow
$d_a, d_b$		Tow diameter (major axis)
$\tilde{d}_a, \tilde{d}_b$		Tow diameter (major axis) projected along the other tow
$h$		Plate thickness
$H$		Unit cell height
$L_a, L_b$		Tow undulation wavelength
$L$		Unit cell length
$t_a, t_b$		Tow thickness (minor axis)
$u_a, u_b$		Tow undulation height
$V_f$		Fiber volume fraction (fiber to tow)
$V_t$		Tow volume fraction (tow to RUC)
$V, V_m$		Total, matrix volumes
$V_a, V_b$		Tow volumes
$W$		Unit cell half-width
$\alpha$		In-plane tow rotation angle
$\beta$		Undulation angle
$\theta$		Bias tow angle
$\phi$		Unit cell orientation angle
<i>Subscript</i>		
$a$		Axial tow
$b$		Bias tow
$m$		Matrix
$t$		Tow

---

<sup>\*</sup>PhD Candidate, Department of Aerospace Engineering.

<sup>†</sup>Professor, Department of Aerospace Engineering.

<sup>‡</sup>Associate Professor, Department of Aerospace Engineering.

## I. Introduction

In aircraft design, aeroelastic tailoring is the application of passive control in the design of the structure to produce favorable deformations through the use of directional stiffness.<sup>1</sup> When this is achieved, there is a synergistic coupling between aerodynamics and structures that contributes to overall performance benefits. The application of aeroelastic tailoring to wing design has been considered for decades, and studies in the literature show varying degrees of success, with most making use of composite materials.

Librescu and Song<sup>2</sup> were one of the first to apply aeroelastic tailoring to composite wings by varying ply angles in thin-walled composite beams. The additional flexibility in transverse shear from using composite materials amplified the wash-in effects of forward sweep, which was found to contribute to the impact of aeroelastic tailoring on the divergence speeds of forward swept wings. Eastep et al.<sup>3</sup> performed aeroelastic tailoring with strength and flutter constraints on wings modeled with composite skins. They used  $[0^\circ, 90^\circ, \pm 45^\circ]$  laminates and optimized the relative proportions of each ply for a range of layup orientations. Their conclusion was that the effect of aeroelastic tailoring in this case was limited because the optimal designs were relatively insensitive to layup orientation when multiple structural constraints were considered. However, a single layup orientation angle was used for the entire structure and only thicknesses were optimized individually for each element in the top and bottom skins, so the design flexibility afforded for aeroelastic tailoring was not significant. Weisshaar and Duke<sup>4</sup> performed aeroelastic tailoring using a laminated box beam model coupled with a simple aerodynamic model based on horseshoe vortices. One of their results was that the low-speed elliptical lift distribution lost at high speeds was recovered by laminate-induced wash-out through aeroelastic tailoring. Overall, aeroelastic tailoring was found to be more effective at high subsonic speeds, when aeroelastic effects are more dominant. Guo et al.<sup>5</sup> performed a similar study using beam elements and found that aeroelastic tailoring is the most effective for unswept wings.

The studies mentioned above report varying levels of performance improvements gained through aeroelastic tailoring with the common theme that flutter and divergence speeds are significantly affected, but the overall weight is relatively insensitive to the design variables. However, the low impact on weight is due to the lack of variables with which to optimize and the corresponding lack of fidelity in the structural model. For instance, the fact that Eastep et al. found aeroelastic tailoring to have negligible effect was likely due to the fact that the single layup orientation design variable was applied to the entire skin and the ply angles were not actually varied. To address this shortcoming, what is desired is a high-fidelity model with the flexibility to design each plate element individually and optimize configuration-level variables simultaneously. With a detailed structural model and a high-fidelity aerodynamics model, a proper study on the potential impact of aeroelastic tailoring can be performed, and it is expected that the result will be a framework that can truly exploit the subtleties of aeroelastic coupling. Only recently, computing power and algorithms have advanced to a point where this is feasible.

Kennedy and Martins<sup>6</sup> proposed a multi-level aerostructural optimization framework incorporating a panel-level weight minimization problem within a system-level optimization problem with aircraft performance objectives. This framework couples a 3-D panel code and a shell-element structures code with a coupled adjoint for sensitivity analysis, and it handles a large number of state variables (97236 structural degrees of freedom and 9440 aerodynamic panels) through efficient parallelization and a large number of design variables (446) using an efficient gradient-based optimizer. This level of fidelity is required to have the design flexibility for effective aeroelastic tailoring.

In this approach, the panel-level design variables parametrize the geometry of stiffeners; however, the ability to parametrize the plate itself would significantly enhance the design freedom. Textile composites represent a class of fiber-reinforced materials whose constituents are the matrix and fibers, arranged in a regular pattern. As with straight-ply laminates, textile composites have more design flexibility than isotropic materials due to their geometric complexity. However, textile composites have three significant advantages over straight-ply laminates. First, their resistance to impact loading is significantly greater because of the geometry of the weaving patterns.<sup>7</sup> This is a significant issue with the use of straight-ply laminates because impacts during flight or maintenance on an aircraft can cause delamination, which is much more difficult to detect than with metal. Secondly, textile composites have properties that are naturally more balanced, which is beneficial when unexpected or unusual loading conditions arise. With straight-ply laminates, a large number of layers are required to achieve the same balance, reducing their advantage in strength-to-weight ratio. The third major benefit is that if a single layer is used — as is the case here — stretching, shear, bending, and twisting are fully decoupled whereas all four are coupled in general for straight-ply laminates, and only in-plane to out-of-plane coupling is removed with a symmetric laminate. An additional benefit for

textile composites is the ease and low cost of manufacturing because of the advanced processes developed in the textile industry.

Among textile composites, 2-D triaxial braided composites (2DTBC) are examined in this work because of the combination of design flexibility and simplicity. 2-D woven composites have fiber tows in only the  $0^\circ$  and  $90^\circ$  directions, so the design freedom is limited. 3-D woven and braided composites, as well as knitted and stitched composites, are not as well understood and the potential for analytical modeling is limited. Furthermore, their tows undulate significantly more out-of-plane, weakening stiffness, whereas 2DTBCs represent a good mixture of structural efficiency and balanced properties.

## II. Multi-Scale Modeling and Design

The overall modeling approach involves multiple physical scales, as illustrated in Figure 1. The first is the molecule level, where molecular dynamics simulations for predicting elastic constants is an ongoing area of research. This scale of modeling is not considered for the current framework. The second is the tow level, in which the transversely isotropic properties of the tow are computed based on the properties of the constituent bundle of fibers and matrix material. The concentric cylinders model (CCM) is used here, with the fiber volume fraction representing the packing efficiency of the tow — i.e. the ratio between total fiber area and tow area for a given cross section. The representative unit cell (RUC) is the smallest repeating pattern in the textile composite. Given a tow volume fraction — the ratio between total tow volume and total RUC volume — and an assumed RUC geometry, the objective here is a model predicting the full 3-D stiffness matrix for the RUC idealized as a homogeneous entity. In this paper, only 2-D triaxial braided composites are considered, and the derivation for the corresponding micromechanical model is presented in a later section. The fourth level is the plate level, at which the RUCs for the constituent layers are assembled to obtain the constitutive relations for the plate in terms of thickness-averaged quantities. The expressions are greatly simplified in the current approach since only one layer is used. Finally, the matrices representing the constitutive relations for the plate are used in the thin-walled finite element model of the structure.

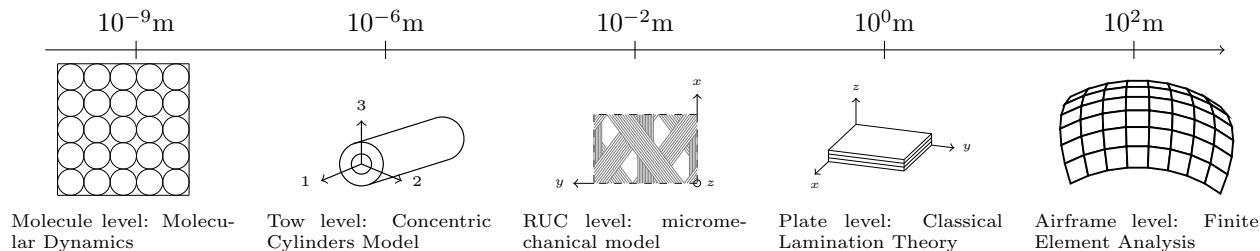


Figure 1: Diagram representing how molecules, fibers, tows, braids, plates, and structures are built up in sequence through a series of models.

A suggested multi-scale optimization process is shown in Figure 2. The fiber and matrix materials are fixed; thus, tow and matrix stiffness matrices are also constant during optimization. Axial tow area, bias tow area, and bias tow angle are the design variables in the micromechanical model while unit cell orientation and plate thickness are the design variables at the classical lamination theory (CLT) level.

A possible sequence of events is discussed briefly. For the first iteration, an initial guess is made for all five variables for each plate element since the stresses are unknown. The linear system from finite element analysis (FEA) is solved and the thickness-averaged stresses are calculated for each plate element. Using these, the optimal unit cell orientation, tow areas, and bias tow angle are computed for each plate and used in the next FEA solve. If the local variables are updated in this manner simultaneously with the system-level optimization problem — involving variables using as sweep and span — it is likely that convergence will require more iterations or it may never converge to the desired tolerance. In that case, there are two options. First, the local variables can simply be considered as part of the system-level optimization, though that significantly increases the number of design variables and may create local minima in the system-level problem. The second option is to separate the convergence of the system-level and plate-level variables. This option is similar to the multidisciplinary feasible (MDF) architecture in multidisciplinary design optimization (MDO) since the coupling between design variables of different plates is fully resolved within a single iteration of the system-level optimization problem.

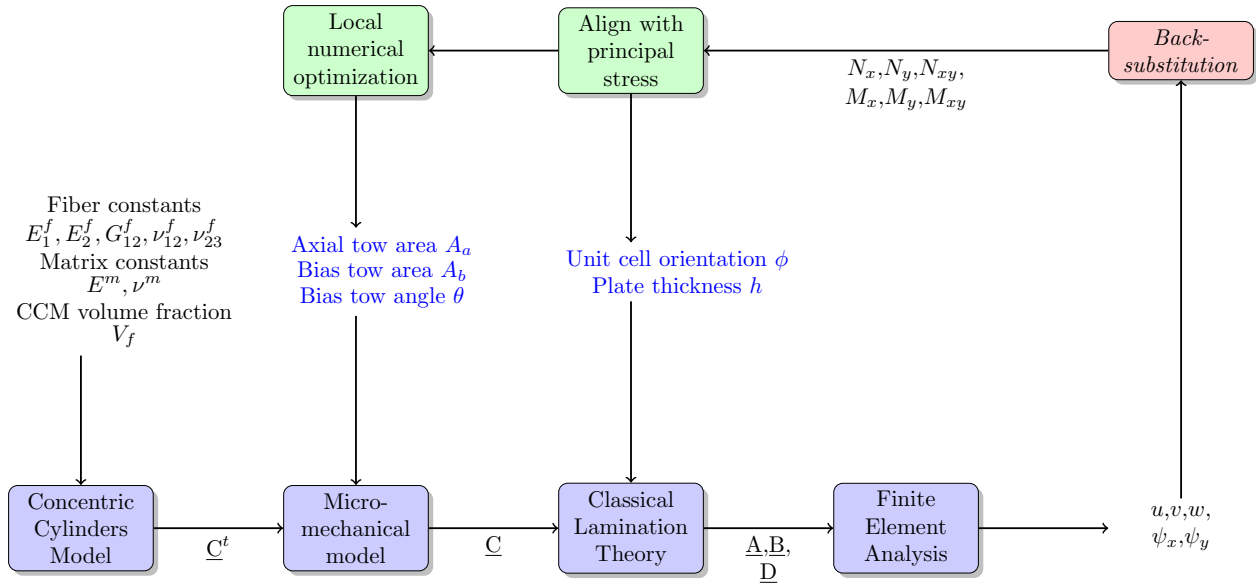


Figure 2: Flowchart for optimization of the plate-level design variables. Based on the loads from the previous FEA solve, the unit cell orientation is computed so that the axial tows are aligned with the largest principal stress. Similarly, optimal axial tow area, bias tow area, and bias tow angle are all computed for each plate element through numerical optimization. This process is repeated until the design variables converge.

### III. Analytical Model

The representative unit cell is the smallest repeating unit in the 2DTBC architecture, shown in Figure 3. An RUC contains two wavelengths of the axial tow aligned with the unit cell coordinate frame as well as one wavelength each of the  $+\theta^\circ$  and  $-\theta^\circ$  bias tows. The axial and bias tow undulations are shown in Figure 4.

The RUC has a height  $H$ , length  $L$ , and width  $2W$ , where  $W$  is the distance between two adjacent axial tows. The axial and bias tow areas, diameters, and thicknesses are represented by  $A_a$ ,  $A_b$ ,  $d_a$ ,  $d_b$ ,  $t_a$ , and  $t_b$ . The axial tow area and diameter in the plane of the bias tow undulation are  $\tilde{A}_a$  and  $\tilde{d}_a$ ; likewise, the bias tow area and diameter in the plane of the axial tow undulation are  $\tilde{A}_b$  and  $\tilde{d}_b$ . The relationships between these RUC dimensions are

$$L_a = \frac{W}{\tan \theta} \quad (1) \quad d_a = \tilde{d}_a \sin \theta \quad (2) \quad A_a = \tilde{A}_a \sin \theta \quad (3) \quad A_a = \pi \frac{d_a t_a}{2} \quad (4)$$

$$L_b = \frac{2W}{\sin \theta} \quad (5) \quad d_b = \tilde{d}_b \sin \theta \quad (6) \quad A_b = \tilde{A}_b \sin \theta \quad (7) \quad A_b = \pi \frac{d_b t_b}{2} \quad (8)$$

The following description of the analytical model consists of two parts: the tow arrangement optimization, which predicts the geometry of the RUC, and the micromechanical model, which estimates the full 3-D stiffness matrix using the modeled geometry.

#### III.A. Tow arrangement optimization

One of the requirements for design optimization with textile composites is a model for the tow geometry as a function of the design variables. For any combination of  $A_a$ ,  $A_b$ , and  $\theta$ , we want to be able to compute undulation amplitudes  $u_a$  and  $u_b$  as well as tow cross-sectional properties. The most accurate approach would be to perform a simulation of the textile process used in manufacturing, considering the full geometries of the tows — including their tendency to twist and deform — while applying tensile loads to tighten the braid as is done in reality. Miao et al.<sup>8</sup> implemented such an approach, using a digital element model to obtain a precise prediction of the tow geometry and correctly capturing the twisting effect due to interaction between tows. Here, we desire closed-form expressions describing the tow geometry — in other words, an analytical solution to the following optimization problem:

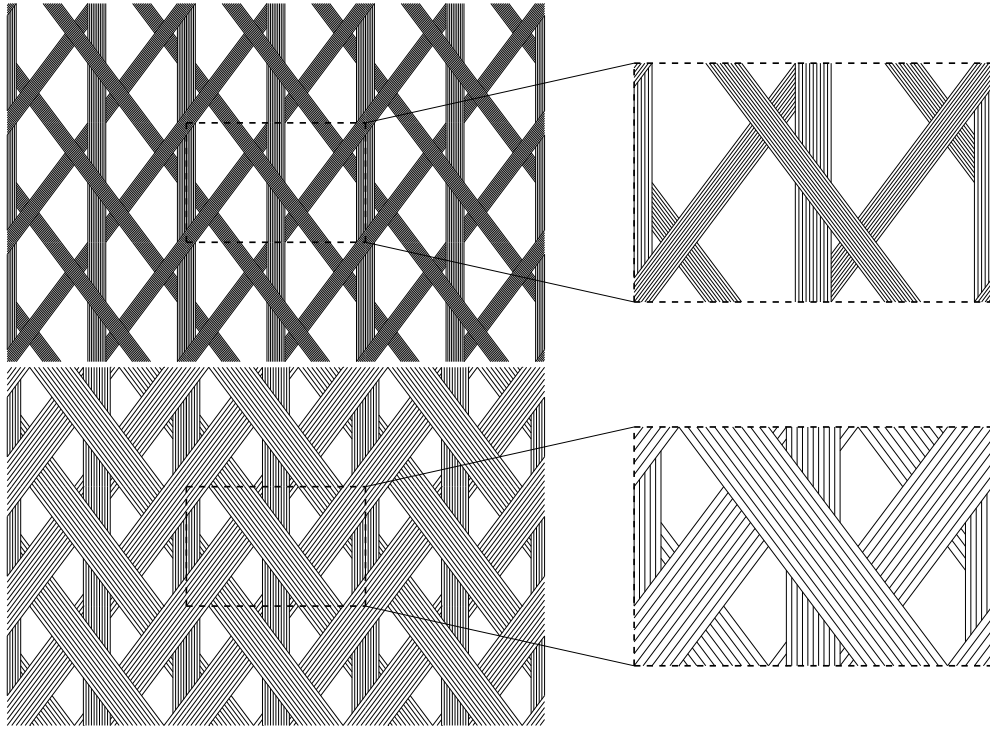


Figure 3: The 2DTBC architecture and its representative unit cell for small diameter tows (top) and large diameter tows (bottom).

$$\begin{aligned}
 & \text{maximize} && \text{RUC fiber density} \\
 & \text{with respect to} && [d_a, d_b, u_a, u_b]^T \\
 & \text{subject to} && \text{inequality constraints enforcing geometric compatibility}
 \end{aligned}$$

The optimization problem essentially solves a packing problem, reflecting actual manufacturing processes which attempt to maximize the fiber volume fraction. Since the fiber and matrix densities are typically on the same order but the fiber is much stiffer, particularly in the axial direction, it is productive to increase the fiber volume fraction as much as possible.

The above optimization problem can be quantified by assuming that the tows cross sections are always elliptical (the tows do not deform) and that their undulation path is periodic with no twist. Still, it is too complex to solve analytically because of the inequality constraints that ensure compatibility. This issue can be resolved by making the following assumptions:

1.  $u_a = 0$
2.  $d_a + \frac{d_b}{\cos \theta} = W$
3.  $u_b = \frac{t_a}{2} + \frac{t_b}{2}$

The first simplification is the assumption that the axial tows do not undulate. Typically, the axial tow is aligned with the direction in which the axial stress is the largest, so the axial tow is also the largest in area and stiffest. More importantly, the wavelength of the axial tow is less than half of that of the bias tow, which makes the axial tow tend to be more flat because any undulation would yield a relatively large spatial frequency. This assumption has been made in other models in the literature with good results.<sup>9</sup> Qualitatively, the second simplification is simply a statement that, during the textile process, the axial and bias tows will widen until they are in contact with each other. Since the number of fibers in a tow is fixed, the tow areas are also roughly constant, so the tendency of the tows to flatten in order to decrease their undulation amplitudes results in a corresponding increase in tow diameters. The final simplification

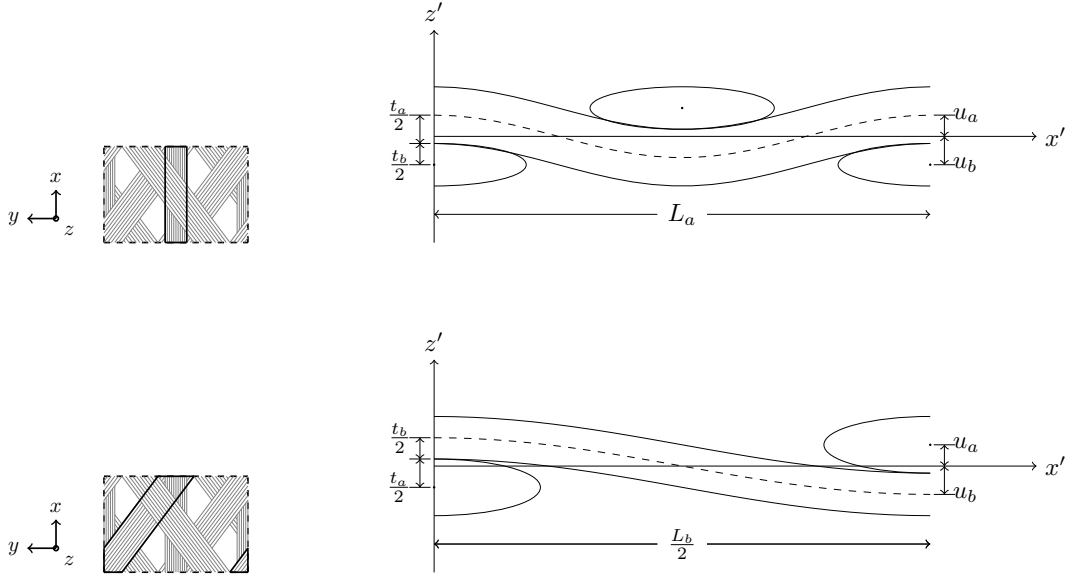


Figure 4: Side view of the axial (top) and bias (bottom) tows. Note the elliptical cross-sectional shapes of the tows and the sinusoidal undulation of the tows. The analytical model simplifies the sinusoidal undulation as a piecewise quadratic.

is obvious from Figure 4. At the points at which the axial and bias tow cross over each other, the bias tow undulation height is its undulation amplitude, which must be equal to half of the sum of the two tow thicknesses since the bias tow would never undulate more than necessary.

With these simplifications, the analytical solution to the tow geometry optimization problem is

$$d_a = \frac{W}{1 + \sqrt{\frac{A_b}{A_a \cos \theta}}} \quad (9) \quad d_b = \frac{W}{1 + \sqrt{\frac{A_a \cos \theta}{A_b}}} \quad (10)$$

$$u_b = \frac{2}{\pi} \left[ \frac{A_a}{W} \left( 1 + \sqrt{\frac{A_b}{A_a \cos \theta}} \right) + \frac{A_b}{W \cos \theta} \left( 1 + \sqrt{\frac{A_a \cos \theta}{A_b}} \right) \right]. \quad (11)$$

This solution gives closed-form expressions for tow diameters and undulation amplitudes ( $u_a = 0$ ) as a function of axial tow area, bias tow area, and bias tow angle. Note that if  $A_b = A_a \cos \theta$ , then  $d_a = d_b = \frac{W}{2}$ , so the two tows share the available width equally. As one of the tow areas increases, more of the available width is allocated to that tow, while the bias tow diameter increases as bias tow angle increases.

### III.B. Micromechanical model

The objective is an analytical model that predicts the stiffness matrix of the RUC, based on the tow geometry optimization results. Analytical micromechanical models for textile composites have been studied for decades, starting with Ishikawa and Chou.<sup>10</sup> They presented three models for 2-D woven composites — the ‘mosaic model’, the ‘fiber undulation model’, and the ‘bridging model’. The first is a 1-D model that assembles cross-ply laminates either in series (iso-stress) or in parallel (iso-strain), the second introduces tow undulation, and the third is a 2-D model that considers undulation in only one direction. Naik and Ganesh<sup>11</sup> later developed fully 2-D models that consider fiber undulation and continuity in both in-plane directions through a CLT-based approach as well. These models were shown to agree well with results from finite element analysis; however, they are limited to prediction of in-plane properties as they are not 3-D models.

To overcome this limitation and obtain the full  $6 \times 6$  stiffness matrix, a 3-D computation of elastic properties is necessary. Sheng and Hoa<sup>12</sup> presented a general approach for deriving the micromechanical model of any RUC from energy methods. For the iso-strain assumption, they derived the volume-averaged stiffness matrix by summing the total potential energy of the RUC to obtain the upper bound for stiffness; for the iso-stress assumption, they derived the volume-averaged compliance matrix by summing the total

complementary potential energy to obtain the lower bound for stiffness. By applying this approach to 2-D woven composites and comparing with experimental results, they found that the iso-strain assumption is more appropriate because the experimental data is much closer to the upper bound than the lower bound. In fact, the upper bound was found to be a good estimate of the actual properties obtained through experiment.

Quek et al.<sup>9</sup> took a similar approach, using the iso-strain assumption to derive a 3-D micromechanical model. Their approach computes the equivalent stiffness matrices as if the entire RUC were made of each of the constituents (axial, bias tow, and matrix), and computes the weighted average based on the respective volume fractions. The results showed good agreement with experiment as well, suggesting the approaches of Sheng and Hoa and Quek et al. are both adequate models for the prediction of RUC elastic properties.

The approach adopted here is based on that of Sheng and Hoa, but the concentric cylinders model is used, as is done by Quek et al., to obtain the properties of the tow. The total potential energy of the RUC is given by

$$\int_V U dV = \int_{V_a} U_a dV_a + \int_{V_{b_+}} U_{b_+} dV_{b_+} + \int_{V_{b_-}} U_{b_-} dV_{b_-} + \int_{V_m} U_m dV_m. \quad (12)$$

Since we are assuming a state of constant strain, all terms can be written as  $U = \frac{1}{2} \underline{\epsilon}^T \underline{C} \underline{\epsilon}$ , so we can remove the common strain terms from the respective integrals, resulting in

$$\begin{aligned} \int \underline{C} dV = & 2 \int \underline{C}^t A_a dx + \int \underline{\mathbb{T}}_{-\theta}^T \underline{\mathbb{T}}_{\beta}^T \underline{C}^t \underline{\mathbb{T}}_{\beta} \underline{\mathbb{T}}_{-\theta} A_b ds \\ & + \int \underline{\mathbb{T}}_{\theta}^T \underline{\mathbb{T}}_{\beta}^T \underline{C}^t \underline{\mathbb{T}}_{\beta} \underline{\mathbb{T}}_{\theta} A_b ds + \int \underline{C}^m dV_m. \end{aligned} \quad (13)$$

Many studies in literature model the undulation path as a sinusoid, but approximating it as a piecewise quadratic simplifies analytical evaluation of the integrals in this case. Since the undulation path is related to  $\beta$  by  $\frac{\partial z'}{\partial x'} = \tan \beta$ , we have

$$z' = u_b \left[ 1 - \left( \frac{2 \sin \theta}{W} x \right)^2 \right] \quad (14)$$

$$ds = \left| \sqrt{1 + \left( \frac{\partial z'}{\partial x'} \right)^2} \right| dx' = \left( \frac{W^2}{8u_b \sin^2 \theta} \right) \sec^3 \beta d\beta. \quad (15)$$

To evaluate the integrals for the volume-averaged stiffness, a coordinate transformation is performed so that  $\beta$  is the variable of integration. The bounds are  $-\beta_0$  and  $\beta_0$ , where  $\beta_0 = \tan^{-1} \left( \frac{4u_b \sin \theta}{W} \right)$ , which is half of the original integral, so the integrand must be doubled. The expression for the  $6 \times 6$  homogenized RUC stiffness matrix is

$$\begin{aligned} \underline{C} = & \frac{2V_a}{V} \underline{C}^t + \frac{W^2}{8u_b \sin^2 \theta} \frac{A_b}{V} \underline{\mathbb{T}}_{-\theta}^T \left[ \int_{-\beta_0}^{\beta_0} \underline{\mathbb{T}}_{\beta}^T \underline{C}^t \underline{\mathbb{T}}_{\beta} 2 \sec^3 \beta d\beta \right] \underline{\mathbb{T}}_{-\theta} \\ & + \frac{W^2}{8u_b \sin^2 \theta} \frac{A_b}{V} \underline{\mathbb{T}}_{\theta}^T \left[ \int_{-\beta_0}^{\beta_0} \underline{\mathbb{T}}_{\beta}^T \underline{C}^t \underline{\mathbb{T}}_{\beta} 2 \sec^3 \beta d\beta \right] \underline{\mathbb{T}}_{\theta} + \frac{V_m}{V} \underline{C}^m, \end{aligned} \quad (16)$$

where  $V_b = \frac{2u_b}{r^2} A_b c_0 s_0$  and  $V_a = \frac{A_a W}{\tan \theta} (c_0 s_0 \text{ is defined later})$ . The  $\underline{\mathbb{T}}$  matrices in the above equations are strain transformation tensors in matrix form. The directions of the transformations are shown in Figure 5. They are given as follows:

$$\underline{\mathbf{T}}_\phi = \begin{bmatrix} \cos^2 \phi & \sin^2 \phi & 0 & 0 & 0 & \cos \phi \sin \phi \\ \sin^2 \phi & \cos^2 \phi & 0 & 0 & 0 & -\cos \phi \sin \phi \\ 0 & 0 & 1 & 0 & 0 & 0 \\ 0 & 0 & 0 & \cos \phi & -\sin \phi & 0 \\ 0 & 0 & 0 & \sin \phi & \cos \phi & 0 \\ -2 \cos \phi \sin \phi & 2 \cos \phi \sin \phi & 0 & 0 & 0 & \cos^2 \phi - \sin^2 \phi \end{bmatrix} \quad (17)$$

$$\underline{\mathbf{T}}_\alpha = \begin{bmatrix} \cos^2 \alpha & \sin^2 \alpha & 0 & 0 & 0 & -\cos \alpha \sin \alpha \\ \sin^2 \alpha & \cos^2 \alpha & 0 & 0 & 0 & \cos \alpha \sin \alpha \\ 0 & 0 & 1 & 0 & 0 & 0 \\ 0 & 0 & 0 & \cos \alpha & \sin \alpha & 0 \\ 0 & 0 & 0 & -\sin \alpha & \cos \alpha & 0 \\ 2 \cos \alpha \sin \alpha & -2 \cos \alpha \sin \alpha & 0 & 0 & 0 & \cos^2 \alpha - \sin^2 \alpha \end{bmatrix} \quad (18)$$

$$\underline{\mathbf{T}}_\beta = \begin{bmatrix} \cos^2 \beta & 0 & \sin^2 \beta & 0 & \cos \beta \sin \beta & 0 \\ 0 & 1 & 0 & 0 & 0 & 0 \\ \sin^2 \beta & 0 & \cos^2 \beta & 0 & -\cos \beta \sin \beta & 0 \\ 0 & 0 & 0 & \cos \beta & 0 & -\sin \beta \\ -2 \cos \beta \sin \beta & 0 & 2 \cos \beta \sin \beta & 0 & \cos^2 \beta - \sin^2 \beta & 0 \\ 0 & 0 & 0 & \sin \beta & 0 & \cos \beta \end{bmatrix}. \quad (19)$$

$$\underline{\epsilon}'' = \underline{\mathbf{T}}_\beta \underline{\epsilon}' \qquad \underline{\epsilon}' = \underline{\mathbf{T}}_\alpha \underline{\epsilon} \qquad \underline{\epsilon} = \underline{\mathbf{T}}_\phi \underline{\epsilon}^*$$

Undulation frame ← Tow frame ← RUC frame ← Plate frame

Figure 5: The tensorial strain transformation matrices relate strains in the plate, RUC, tow, and undulation frames.  $\alpha$  is a rotation in the negative sense in a right-handed coordinate system, reflecting the definition of positive  $\theta$ .

The integrals in the expression for the  $6 \times 6$  homogenized RUC stiffness matrix are evaluated analytically. The matrix products in the integrand are evaluated first to obtain the tow stiffness matrix in the tow undulation frame with the undulation angle  $\beta$  removed, yielding expressions involving the transversely isotropic stiffness constants of the tow multiplied by fourth order sine and cosine terms. These are then multiplied by  $\sec^3 \beta$ , which arises from the transformation from  $ds$  to  $d\beta$ . Among these, all odd terms can be ignored since they are zero when integrated from  $-\beta_0$  to  $\beta_0$ , and the even terms are integrated analytically.

For convenience, two variables are introduced,  $r = \frac{4u_b \sin \theta}{W}$  and  $r' = \sqrt{1 + r^2}$ . The integrated expressions



for each trigonometric term are

$$c4 = \frac{4r}{r'} \quad (20)$$

$$c2s2 = \frac{-4r}{r'} + 2 \ln \left( \frac{1 + \frac{r}{r'}}{1 - \frac{r}{r'}} \right) \quad (21)$$

$$s4 = \frac{4r}{r'} + \frac{1}{1 - \frac{r}{r'}} - \frac{1}{1 + \frac{r}{r'}} - \frac{7}{4} \ln \left( 1 + \frac{r}{r'} \right) + \frac{3}{2} \ln \left( 1 - \frac{r}{r'} \right) \quad (22)$$

$$c2 = 2 \ln \left( \frac{1 + \frac{r}{r'}}{1 - \frac{r}{r'}} \right) \quad (23)$$

$$s2 = 2rr' - \ln \left( \frac{1 + \frac{r}{r'}}{1 - \frac{r}{r'}} \right) \quad (24)$$

$$c0s0 = 2rr' + \ln \left( \frac{1 + \frac{r}{r'}}{1 - \frac{r}{r'}} \right), \quad (25)$$

where  $c4 = 2 \int_{-\beta_0}^{\beta_0} \cos^4 \beta \sec^3 \beta d\beta$ , as an example. Then, the integrated stiffness matrix in the  $\mathcal{F}'$  frame is

$$2 \int_{-\beta_0}^{\beta_0} \underline{\mathbf{U}}_{\beta}^T \underline{\mathbf{C}}^t \underline{\mathbf{U}}_{\beta} \sec^3 \beta d\beta = \begin{bmatrix} C'_{11} & C'_{12} & C'_{13} & 0 & 0 & 0 \\ C'_{12} & C'_{22} & C'_{23} & 0 & 0 & 0 \\ C'_{13} & C'_{23} & C'_{33} & 0 & 0 & 0 \\ 0 & 0 & 0 & C'_{44} & 0 & 0 \\ 0 & 0 & 0 & 0 & C'_{55} & 0 \\ 0 & 0 & 0 & 0 & 0 & C'_{66} \end{bmatrix} \quad (26)$$

$$C'_{11} = C_{11}^t c4 + (2C_{12}^t + 4C_{55}^t) c2s2 + C_{22}^t s4 \quad (27)$$

$$C'_{12} = C_{12}^t c2 + C_{23}^t s2 \quad (28)$$

$$C'_{13} = C_{12}^t c4 + (C_{11}^t + C_{22}^t - 4C_{55}^t) c2s2 + C_{12}^t s4 \quad (29)$$

$$C'_{22} = C_{22}^t c0s0 \quad (30)$$

$$C'_{23} = C_{23}^t c2 + C_{12}^t s2 \quad (31)$$

$$C'_{33} = C_{22}^t c4 + (2C_{12}^t + 4C_{55}^t) c2s2 + C_{11}^t s4 \quad (32)$$

$$C'_{44} = C_{44}^t c2 + C_{66}^t s2 \quad (33)$$

$$C'_{55} = C_{55}^t c4 + (C_{11}^t - 2C_{12}^t + C_{22}^t - 2C_{55}^t) c2s2 + C_{55}^t s4 \quad (34)$$

$$C'_{66} = C_{66}^t c2 + C_{44}^t s2. \quad (35)$$

## IV. Application

### IV.A. Validation

Table 1 compares the results obtained from the current model with those obtained experimentally and analytically by Kier et al.<sup>13</sup> In general, the current model does not agree as well as the Quek model with one notable exception. The experimentally measured  $G_{xy}$  constant increases with increasing bias tow angle, which is captured by the current model, but the opposite is true with the Quek model. It is hypothesized that this difference is caused by the fact that the current model correctly predicts that with increasing bias tow angle, the bias tow undulation increases, increasing the RUC volume and increasing the relative amount of matrix in the RUC. Since the matrix material makes a larger contribution to in-plane shear stiffness, this trend offsets the influence of the bias tow contribution, which changes as the bias tow angle varies.

Overall, the current model is not as accurate as existing models, but the key difference is that the current model computes the tow geometry automatically, with only tow areas, bias tow angle, and fiber volume fraction required as input variables. Existing models require many more variables to be experimentally measured to be able to compute the stiffness matrix. With the current model, the trends were predicted satisfactorily, and optimization is possible with this new model.

30°	Experimental	Quek	Current
$E_x$ [GPa]	$53.1 \pm 0.8$	58.3	50.5
$E_y$ [GPa]	$7.3 \pm 0.5$	8.06	9.19
$G_{xy}$ [GPa]	$8.3 \pm 2.5$	10.8	9.45
$\nu_{xy}$	0.93	0.995	0.76
$G_{yx}$ [GPa]	$15.4 \pm 3.2$		
45°	Experimental	Quek	Current
$E_x$ [GPa]	$27.9 \pm 1.1$	29.4	30.3
$E_y$ [GPa]	$13.7 \pm 1.2$	13.9	17.6
$G_{xy}$ [GPa]	$10.8 \pm 2.0$	9.35	9.79
$\nu_{xy}$	0.59	0.535	0.49
$G_{yx}$ [GPa]	$14.4 \pm 4.0$		
60°	Experimental	Quek	Current
$E_x$ [GPa]	$23.2 \pm 0.8$	28.4	27.0
$E_y$ [GPa]	$22.1 \pm 0.1$	22.6	26.9
$G_{xy}$ [GPa]	$11.8 \pm 2.7$	8.85	10.9
$\nu_{xy}$	0.30	0.328	0.31
$G_{yx}$ [GPa]	$11.9 \pm 1.3$		

Table 1: Comparison between the results from the current analytical model and the analytical results from Quek’s model and experimental results presented in Kier et al.<sup>13</sup>

#### IV.B. Optimization Problem

For a single-layer homogeneous laminate, bending and stretching are not coupled and the vector of loads  $\underline{\mathbf{N}}$  and  $\underline{\mathbf{M}}$  can be combined to form a single vector that induces a maximum in-plane strain of  $\epsilon$ :

$$\begin{Bmatrix} \underline{\mathbf{N}} \\ \underline{\mathbf{M}} \end{Bmatrix} = \begin{bmatrix} \underline{\mathbf{A}} & \mathbf{0} \\ \mathbf{0} & \underline{\mathbf{D}} \end{bmatrix} \begin{Bmatrix} \underline{\epsilon}^0 \\ \underline{\kappa} \end{Bmatrix} \quad (36)$$

$$\underline{\epsilon}^0 = \underline{\mathbf{A}}^{-1} \underline{\mathbf{N}} = \frac{1}{h} \underline{\mathbf{C}}^{-1} \underline{\mathbf{N}} \quad (37)$$

$$\underline{\kappa} = \underline{\mathbf{D}}^{-1} \underline{\mathbf{M}} = \frac{12}{h^3} \underline{\mathbf{C}}^{-1} \underline{\mathbf{M}} \quad (38)$$

$$\underline{\epsilon} = \underline{\epsilon}^0 + z \underline{\kappa} = \frac{1}{h} \underline{\mathbf{C}}^{-1} \left( \underline{\mathbf{N}} + z \frac{12}{h^2} \underline{\mathbf{M}} \right). \quad (39)$$

The general optimization problem is

$$\begin{aligned} & \text{minimize} && \text{RUC areal density} \\ & \text{with respect to} && [\theta, h, \phi, A_a, A_b]^T \\ & \text{subject to} && \text{tow strains less than 0.005} \\ & && \text{matrix shear stress less than 5 MPa} \end{aligned}$$

The tow strains are very insensitive to the magnitudes of  $A_a$  and  $A_b$ , so the plate thickness,  $h$ , is an important variable for scaling the problem based on the magnitudes of the loads applied. The remaining degrees of freedom —  $\theta$ ,  $\phi$ , and  $A_a/A_b$  — all have a similar effect of redistributing stiffness among the various components as opposed to changing its effective magnitude.

To simplify the problem, it is assumed here that only in-plane stresses are applied.  $\phi$  can be chosen to align the RUC with the principal directions such that the axial tow is parallel to the largest principal stress. This yields a new  $N_x$  and  $N_y$  in the RUC frame with no shear stress component. If we denote  $N_x^*$ ,  $N_y^*$ , and

$N_{xy}^*$  the stresses in the original plate frame, we have  $\phi = \frac{1}{2} \tan^{-1} \frac{2N_{xy}^*}{N_x^* - N_y^*}$  and the tow strains can be found using

$$\begin{Bmatrix} \epsilon_a \\ \epsilon_b \end{Bmatrix} = \begin{bmatrix} 1 & 0 \\ \cos^2 \theta & \sin^2 \theta \end{bmatrix} \begin{Bmatrix} \epsilon_x \\ \epsilon_y \end{Bmatrix} \quad (40)$$

$$\begin{Bmatrix} \epsilon_a \\ \epsilon_b \end{Bmatrix} = \frac{1}{h} \begin{bmatrix} 1 & 0 \\ \cos^2 \theta & \sin^2 \theta \end{bmatrix} \begin{bmatrix} C_{11} & C_{12} \\ C_{12} & C_{22} \end{bmatrix}^{-1} \begin{Bmatrix} N_x \\ N_y \end{Bmatrix} \quad (41)$$

$$\begin{Bmatrix} \epsilon_a \\ \epsilon_b \end{Bmatrix} = \frac{1}{h} \begin{bmatrix} 1 & 0 \\ \cos^2 \theta & \sin^2 \theta \end{bmatrix} \begin{bmatrix} C_{11} & C_{12} \\ C_{12} & C_{22} \end{bmatrix}^{-1} \begin{bmatrix} \cos^2 \phi & \sin^2 \phi & 2 \cos \phi \sin \phi \\ \sin^2 \phi & \cos^2 \phi & -2 \cos \phi \sin \phi \end{bmatrix} \begin{Bmatrix} N_x^* \\ N_y^* \\ N_{xy}^* \end{Bmatrix}. \quad (42)$$

The elastic constants are insensitive to proportional increases to  $A_a$  and  $A_b$ ; however, they are more sensitive to the ratio between the tow areas. From the tow geometry optimization,  $A_a$  must be sufficiently greater than  $A_b$  for the assumption to be valid that the axial tow does not undulate. However, the bias tow area should not be too small as it serves a dual purpose of carrying the loads in the  $y$  direction and providing more balanced stiffness even when  $N_y$  is small for considerations such as impact resistance. For the numerical optimization results that follow, a ratio of 4 is used as a compromise.

#### IV.C. Numerical Optimization

From the previous discussion, the remaining design variables are  $\theta$  and  $h$ .  $\phi$  is used to align the RUC with the principal directions, and the tow areas are chosen to give a ratio of 4. Realistic values for the tow areas are  $A_a/W^2 = 0.08$  and  $A_b/W^2 = 0.02$ . The numerical optimization problem for a given plate with a given loading is then as follows:

$$\begin{array}{ll} \text{minimize} & \text{RUC areal density} \\ \text{with respect to} & [\theta, h/W]^T \\ \text{subject to} & |\epsilon_a| \leq 0.005 \\ & |\epsilon_b| \leq 0.005 \end{array}$$

Since the optimization problem is continuous, it is solved using SNOPT, a Sequential Quadratic Programming (SQP) algorithm that handles nonlinear, convex optimization problems very well.<sup>14</sup> SQP methods define a quadratic sub-problem with linearized constraints at every major iteration, approximating the Hessian matrix with the widely-used BFGS update formula and using a line search along each computed search direction. Here, gradients computed using the finite difference method provide sufficient accuracy — optimality and feasibility are converged to  $10^{-10}$ .

The optimization results are shown in Figure 6. For simplicity, only normal stresses are applied to remove  $\phi$  from the problem, and the applied stresses are  $N_x = 1$  MPa and  $N_y$  between 0 MPa and 1 MPa. Only this range of  $N_y$  values are plotted because  $|N_x| > |N_y|$  by construction. The plate thickness bounds are never active and the lower bound of  $10^\circ$  is active for  $\theta$  for low values of  $N_y/N_x$  because a high transverse stiffness is not required in this range.

Above roughly  $N_y/N_x = 0.2$ , the results are as expected. With increasing  $N_y/N_x$ , the required plate thickness increases since the magnitude of the applied load grows larger.  $\theta$  is also increasing because more and more stiffness is needed in the transverse direction as  $N_y$  increases. From the behavior below roughly  $N_y/N_x = 0.2$ , it is clear that the Lagrangian is multi-modal. There are likely two possible solutions due to the fact that the optimizer can achieve an efficient design with a very low value of  $\theta$  but a thicker plate or with a higher value of  $\theta$  and a lower plate thickness. Evidently, the former option provides a lower areal density for small  $N_y$  whereas the opposite is true for larger  $N_y$  because the increase in plate thickness for the former option is too great due to the larger transverse load.

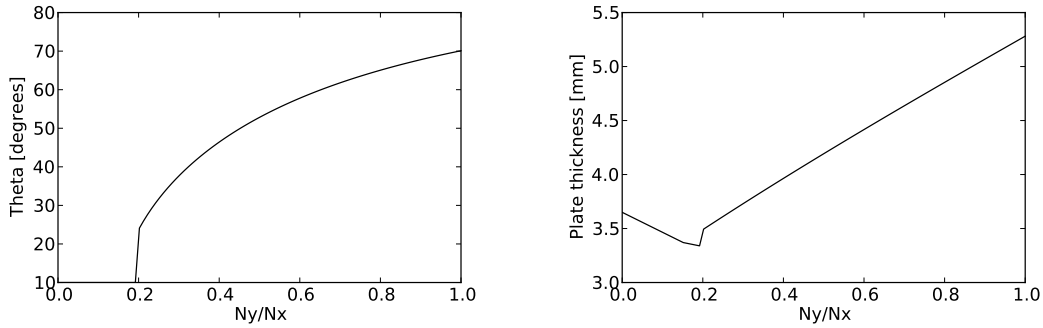


Figure 6: Optimized values of  $\theta$  and  $h$  plotted versus  $N_y/N_x$ . The axial load applied is  $N_x = 1$  MPa.

## V. Conclusion

The model developed in this paper addresses some of challenges associated with performing aeroelastic tailoring with 2-D triaxial braided composites. The RUC geometry is modeled using an optimization formulation for the packing problem which provides a closed form solution that is used as part of the micromechanical model. Existing models require experimental measurement of numerous geometric properties for a given RUC configuration, which prohibits design optimization because these inevitably vary as the design variables change. The micromechanical uses a volume-averaged stiffness approach under the iso-strain assumption, and closed-form solutions are obtained here as well. The computed elastic constants show good agreement with experiment in most cases, and when they do not, the error is likely due to the tow geometry model. Preliminary results from numerical design optimization of the RUC are robust and agree with intuition.

## References

- <sup>1</sup>Shirk, M. H., Hertz, T. J., and Weisshaar, T., “Aeroelastic tailoring — theory, practice, and promise,” *Journal of Aircraft*, Vol. 23, No. 1, 1986, pp. 6–18.
- <sup>2</sup>Librescu, L. and Song, O., “On the static aeroelastic tailoring of composite aircraft swept wings modelled as thin-walled beam structures,” *Composites Engineering*, Vol. 2, No. 5-7, 1992, pp. 497–512.
- <sup>3</sup>Eastep, F. E., Tischler, V. A., Venkayya, V. B., and Khot, N. S., “Aeroelastic Tailoring of Composite Structures,” *Journal of Aircraft*, Vol. 36, No. 6, 1999, pp. 1041–1047.
- <sup>4</sup>Weisshaar, T. and Duke, D., “Induced Drag Reduction Using Aeroelastic Tailoring with Adaptive Control Surfaces,” *Journal of Aircraft*, Vol. 43, No. 1, 2006, pp. 157–164.
- <sup>5</sup>Guo, S., Cheng, W., and Cui, D., “Aeroelastic Tailoring of Composite Wing Structures by Laminate Layup Optimization,” *AIAA Journal*, 2006, pp. 3146–3150.
- <sup>6</sup>Kennedy, G. J. and Martins, J. R. R. A., “Aerostructural design optimization of composite aircraft with stress and local buckling constraints using an implicit structural parametrization,” April 2011.
- <sup>7</sup>Tong, L., Mouritz, A. P., and Bannister, M. K., *3D Fibre Reinforced Polymer Composites*, Elsevier, 2002.
- <sup>8</sup>Miao, Y., Zhou, E., Wang, Y., and Cheeseman, B. A., “Mechanics of textile composites: Micro-geometry,” *Composites Science and Technology*, Vol. 68, No. 7-8, 2008, pp. 1671–1678.
- <sup>9</sup>Quek, S. C., Waas, A. M., Shahwan, K. W., and Agaram, V., “Analysis of 2D triaxial flat braided textile composites,” *International Journal of Mechanical Sciences*, Vol. 45, No. 6-7, 2003, pp. 1077–1096.
- <sup>10</sup>Ishikawa, T. and Chou, T. W., “Stiffness and strength behaviour of woven fabric composites,” *Journal of Materials Science*, Vol. 17, No. 11, 1982, pp. 3211–3220.
- <sup>11</sup>Naik, N. K. and Ganesh, V. K., “Prediction of on-axes elastic properties of plain weave fabric composites Naik, N.K. and Ganesh, V.K. *Composites Science and Technology* Vol 44 No 22 (1992) pp 135152,” *Composites*, Vol. 24, No. 4, 1993, pp. 368–368.
- <sup>12</sup>Sheng, S. Z. and Hoa, S. V., “Three Dimensional Micro-Mechanical Modeling of Woven Fabric Composites,” *Journal of Composite Materials*, Vol. 35, No. 19, 2001, pp. 1701–1729.
- <sup>13</sup>Kier, Z. T., Salvi, A., Theis, G., Waas, A. M., and Shahwan, K., “Predicting Mechanical Properties of 2D Triaxially Braided Textile Composites Based on Microstructure Properties,” 2010.
- <sup>14</sup>Gill, P., Murray, W., and Saunders, M., “SNOPT: An SQP algorithm for large-scale constraint optimization,” *SIAM Journal of Optimization*, Vol. 12, No. 4, 2002, pp. 979–1006.